Differential requirements for the EF-hands of human centrin2 in primary ciliogenesis and nucleotide excision repair

Ebtissal M. Khouj[1], Suzanna L. Prosser[1,2], Haruto Tada[3,4], Weng Man Chong[5], Jung-Chi Liao[5], Kaoru Sugasawa[3,4] and Ciaran G. Morrison[1,*].

[1]Centre for Chromosome Biology, School of Natural Sciences, National University of Ireland Galway, Galway, Ireland, [2]Lunenfeld-Tanenbaum Research Institute, Sinai Health System, 600 University Avenue, Toronto, Ontario M5G 1X5, Canada, [3]Biosignal Research Center and [4]Graduate School of Science, Kobe University, 1-1 Rokkodai-cho, Nada-ku, Kobe, Hyogo 657-8501, Japan and [5]IAMS Academia Sinica, No 1 Roosevelt Rd Sec 4, 10617 Taipei City, Taiwan

Keywords: Primary cilium; centrosome; centriole; centrin2; nucleotide excision repair

***Corresponding author**: Ciaran.Morrison@nuigalway.ie

JCS Advance Online Article. Posted on 6 September 2019

Summary statement

Mutagenesis analysis of human centrin2 reveals a separation of functions whereby centrin2 that is defective in calcium binding can support nucleotide excision repair but not primary ciliogenesis.

Abstract

Centrin2 is a small, conserved calcium-binding protein that localizes to the centriolar distal lumen in human cells. It is required for efficient primary ciliogenesis and nucleotide excision repair (NER). Centrin2 forms part of the xeroderma pigmentosum group C protein complex. To explore how centrin2 contributes to these distinct processes, we mutated the 4 calcium-binding EF-hand domains of human centrin2. Centrin2 in which all EF-hands had been mutated to ablate calcium binding (a '4DA' mutant) was capable of supporting in vitro NER and was as effective as wild-type centrin2 in rescuing the UV sensitivity of centrin2 null cells. However, we found that mutation of any of the EF-hands impaired primary ciliogenesis in hTERT-RPE1 cells to the same extent as deletion of centrin2. Phenotypic analysis of the 4DA mutant revealed defects in centrosome localisation, centriole satellite assembly, ciliary assembly and function and in interactions with POC5 and SFI1. These observations indicate that centrin2 requires calcium-binding capacity for its primary ciliogenesis functions, but not NER, and suggest these functions require that centrin2 be capable of forming complexes with partner proteins.

Introduction

Primary cilia are membrane-bounded, antenna-like structures that arise from the surface of most human cell types to sense and transduce chemical and mechanical signals (Goetz and Anderson, 2010). Defective primary cilium formation or activity causes a complex range of human developmental disorders that affect the kidney, eye, liver, brain and skeleton, collectively termed the ciliopathies (Braun and Hildebrandt, 2017). Furthermore, loss of primary ciliation is commonly seen in cancer and has been suggested as an early step in oncogenesis (Sanchez and Dynlacht, 2016).

The 'stalk' of the cilium, the axoneme, consists of nine doublet microtubules extending from one end of the basal body, a centriole that has docked to the plasma membrane during ciliogenesis (Sorokin, 1962). Centrioles show a striking polarity because of their microtubule-based structure. The minus ends of the centriolar microtubule triplets define the centrioles' proximal ends. At the distal ends, two sets of radially arranged appendages distinguish the older, 'mother' centriole. Distal appendages (DAs), the structures forming 'transition fibres' in basal bodies, are necessary for the mother centriole to act as the basal body during ciliogenesis (Tanos et al., 2013). Reverse genetic experiments have established a core set of DA proteins that constitutively localize to these structures and are required for ciliogenesis (Graser et al., 2007, Tanos et al., 2013). Recent super-resolution imaging of the pinwheel-like blades that comprise the DAs has positioned this core set extending outward from the mother centriole in the following order: CEP83-CEP89-SCLT-CEP164, with FBF1 located between the blades (Yang et al., 2018).

Another crucial requirement for axoneme outgrowth is the removal of CP110 and its partner protein, CEP97, from the mother centriole distal end (Spektor et al., 2007, Tsang et al., 2008). CP110 interacts with components of the centriolar distal lumen, including centrin2, and is

involved in centriole duplication and elongation, acting as a length-regulatory centriole cap (Chen et al., 2002, Tsang et al., 2006, Kleylein-Sohn et al., 2007). Centrosomal-P4.1-associated protein (CPAP) is a tubulin-binding regulator of centriole length (Tang et al., 2009). Overexpression of CPAP increases centriole length, while its depletion impedes centriole duplication and elongation (Tang et al., 2009). CP110 has the reciprocal effect of CPAP in centriole length regulation: its depletion causes centriole lengthening and its overexpression blocks centriole extension (Chen et al., 2002, Spektor et al., 2007). Current models suggest that CP110 may block ciliogenesis by impeding the interaction of CEP290 with Rab8, a small GTPase required for vesicle docking and ciliogenesis. Another CP110 interactor, Talpid3, also contributes to the appropriate regulation of Rab8 during the maturation of the ciliary vesicle (Kobayashi et al., 2014). However, knockout experiments in mouse indicated a requirement for CP110 in subdistal appendage assembly and ciliary vesicle docking (DAs were not examined in this experiment), suggesting that CP110's roles change during ciliogenesis (Yadav et al., 2016). One mechanism that removes CP110 during ciliogenesis involves the CEP164-dependent activation of tau tubulin B kinase (TTBK2) at basal bodies, although the relevant TTBK2 targets are not yet defined (Cajanek and Nigg, 2014, Goetz et al., 2012). Another mechanism controlling CP110 removal involves its ubiquitination and subsequent degradation through the $SCF^{cyclin\ F}$ ubiquitin ligase complex (D'Angiolella et al., 2010). This activity is opposed by the deubiquitinating enzyme, USP33 (Li et al., 2013). The precise details of the activities and regulation of CP110 at specific stages during ciliogenesis remain to be defined.

Centrin2 (also known as caltractin) is a member of a family of small, calmodulin-like proteins that bind calcium through 4 EF-hand domains. They are found in the distal centriolar lumen and in several other locations throughout the cell (Paoletti et al., 1996, Dantas et al., 2012). Centrins are required for centriole formation in lower eukaryotes (Zhang and He, 2011) but, despite some siRNA studies indicating a role in centriole formation in mammalian cells, our

data using gene knockouts in chicken and human cells have shown that centriole duplication is normal in the absence of centrin2 (Dantas et al., 2011, Prosser and Morrison, 2015, Salisbury et al., 2002). Centrin2 is a component of the xeroderma pigmentosum group C complex and ensures efficient nucleotide excision repair (NER) of various helix-distorting DNA lesions (Araki et al., 2001, Nishi et al., 2005, Acu et al., 2010, Dantas et al., 2011, Daly et al., 2016). Interestingly, it is required for normal ciliogenesis in mice and human cells (Graser et al., 2007, Mikule et al., 2007, Prosser and Morrison, 2015, Ying et al., 2014), with its deficiency causing abnormal regulation of the distal end of the mother centriole. How centrin2 contributes to the two processes of NER and primary ciliogenesis is not clear.

Here we have used a mutagenesis approach to dissect the functions of the EF-hands of human centrin2. We find a marked distinction in the requirements for centrin2 calcium binding capacity between NER and primary ciliogenesis. The pronounced requirement for centrin and its EF-hands in primary ciliogenesis suggests that a key role for centrin2 lies in allowing multimeric protein assembly through calcium-dependent conformational shifts.

Results

Analysis of the EF-hands of centrin2 in centriolar localization and DNA damage responses

To explore the functions of the four EF-hands of human centrin, we used site-directed mutagenesis to ablate their calcium-binding capacity. We mutated to alanine the first aspartic acid residue of the loop region of the EF-hands, which is necessary for Ca^{2+} binding (Geiser et al., 1991, Gifford et al., 2007, Vonderfecht et al., 2011), at D41, D77, D114 and D150. We then generated mutants of the N-terminal and C-terminal pairs of EF-hands, and a mutant in which all four EF-hands were mutated ('4DA'). Myc-tagged versions of these mutants, with the exception of the D150A single mutant, and the wild-type centrin2 protein were stably expressed in *CETN2* knockout hTERT-RPE1 cells (Prosser and Morrison, 2015) and we selected clones with expression levels similar to the endogenous protein (Figure 1A). We then tested for the ability of these mutants to localise to centrioles. As shown in Figure 1B, C, single EF-hand mutations were compatible with centriolar localisation, but the mutation of the two C-terminal or all four EF-hands abrogated centrin2 localisation to centrioles.

Notably, despite the impact on centriole localization, a clonogenic survival assay showed that the centrin2 4DA mutant was as capable as wild-type centrin2 at rescuing defective NER in centrin2 null cells (Daly et al., 2016) (Figure 2A). Furthermore, an in vitro assay indicated that the centrin2 4DA mutant was fully capable of stimulating the early stages of NER of 6-4 photoproducts (Figure 2B, C). We next tested whether loss of the EF-hands impacted on the interaction between centrin2 and XPC. As shown in Figure 2D, recombinant 4DA centrin2 was capable of binding to XPC-RAD23B, although somewhat less efficiently than the wild-type protein. Together, these data show that centrin2's roles in NER are independent of the EF-hands.

We next tested whether the centriolar satellites (Tollenaere et al., 2015) were affected by the mutation of the EF-hands of centrin. Notably, mutation of any of the EF-hands caused a decline in PCM1 levels around the centrosome similar to that seen in the *CETN2* null clone (Figure 3A, B). This observation suggests a role for centrin2 in satellite regulation, consistent with the previously-described localisation of centrin to satellites (Loffler et al., 2013, Prosser et al., 2009). Alterations in centriolar satellite density can affect centrosome duplication (Flanagan et al., 2017, Kodani et al., 2015, Loffler et al., 2013, Prosser et al., 2009). Therefore, we quantitated centrosome amplification after ionising (IR) and ultraviolet (UV) irradiation, visualizing centrioles with the proximal end marker CEP135 (Ohta et al., 2002) and centrin3 which is representative of a distinct family of centrins (Figure 3C) (Middendorp et al., 2000). *CETN2* mutants showed similar levels of centriole amplification (3 or >4 centrioles) to wild-type cells, except in the case of the D77A mutants, where there was a moderate reduction (Figure 3D). In general, the *CETN2* mutants showed more cells with 2 centrioles and fewer with 4 than controls after IR and UV, potentially indicating some altered cell cycle distribution. However, IR-and UV-induced phosphorylation of CHK1 and CDK2, modifications that are necessary for DNA damage-induced centrosome amplification (Bourke et al., 2010), were initiated with normal kinetics in centrin2-deficient and centrin2 4DA-expressing cells, suggesting that DNA damage responsive cell cycle checkpoint signalling was unaffected by the loss of centrin2 or its EF-hands (Supplemental Figure 1A, B).

Requirement for the EF-hands of centrin2 in primary ciliogenesis

Our next question concerned the requirement for centrin2 EF-hands in primary cilium formation. To address this, we serum-starved the *CETN2* mutant clones and quantitated primary cilium formation by immunofluorescence microscopy of acetylated tubulin, Arl13B and glutamylated tubulin. As shown in Figure 4A, B, staining for acetylated and glutamylated

tubulin recapitulated previous findings in which we observed a marked deficit in primary cilium formation in the absence of centrin2 (Prosser and Morrison, 2015). None of the EF-hand mutants could rescue primary ciliation, with the D77A and 4DA mutants showing a more severe phenotype than even the null cells. This result was seen in two additional *CETN2* null clones that expressed each mutant, so the impact of D77A and 4DA mutations was not due to individual clonal effects. A more moderate ciliary defect was seen with ARL13B staining of centrin2 mutant cells, again with the D77A and 4DA mutants showing a particularly clear deficiency. As the ARL13B signal reveals the membrane region around the extension of an axoneme, these observations are consistent with compromised stability of the tubulin-based axonemal structure in centrin2 mutants, within an ARL13B-containing ciliary membrane. Notably, those few centrin2 null, D77A and 4DA cells that did make a cilium were markedly deficient in ciliary Hedgehog signalling, with a significantly reduced number of cells being capable of relocalising Smoothened to the cilium upon agonist stimulation (Figure 4C, D). These findings suggest that changes in the EF-hands of centrin strongly affect ciliary integrity and dynamics, as determined by tubulin stability within cilia and by ciliary functioning.

Causes of the ciliary defect seen in the absence of centrin2 include the improper retention of CP110 at the distal end of the mother centriole and the defective localisation of TTBK2 (Prosser and Morrison, 2015). To test if CP110 regulation was affected by mutation of centrin2's EF-hands, we scored CP110 localisation in serum-starved cells and found that mutation of any of the EF-hands impaired CP110 removal after serum starvation, to at least the same extent as was observed in *CETN2* null cells (Figure 5A, B). A key regulator of appropriate TTBK2 localisation is the distal appendage protein, CEP164 (Cajanek and Nigg, 2014, Oda et al., 2014). We used STORM microscopy to visualise CEP164 structures in centrin2-deficient cells and in cells that lack centrobin, another centriolar component whose absence negatively affects CP110 removal and primary ciliogenesis (Betzig et al., 2006,

Heilemann et al., 2008, Rust et al., 2006, Yang et al., 2018, Ogungbenro et al., 2018). As shown in Figure 5C, D, CEP164 formed ninefold patterns with similar radii in wild-type, centrin2 and centrobin null, as well as 4DA cells, suggesting that the distal appendage structures are unaffected by the absence of centrin2 or centrobin, or by the mutation of the EF-hands of centrin2 (Tanos et al., 2013, Yang et al., 2018), We then monitored TTBK2 localisation to mother centrioles and found that cells expressing any of the EF-hand mutants were compromised in localising TTBK2 to the centriole after serum starvation to the same extent as null cells (Figure 5E, F). STORM imaging revealed a marked distortion of TTBK2 in centrin2-deficient cells (Figure 5G, H). Given the abnormal localisation of CEP164 away from the appendages that we have previously noted in *CETN2* null cells (Prosser and Morrison, 2015), these findings show that the localisation of CEP164 to the distal appendages is not sufficient to ensure appropriate TTBK2 localisation. Furthermore, our observations implicate all of the EF-hands of centrin2 in the regulation of CP110 removal and TTBK2 localisation to the distal end of the mother centriole.

Our findings suggest defects in tubulin stability or transport during ciliogenesis in centrin2 mutant cells, rather than problems in vesicle docking (Figures 4A, 4B, 5 and (Prosser and Morrison, 2015)). Therefore, we tested if the length of cilia was affected in centrin2 mutant cells by staining cells with antibodies against acetylated tubulin. We found that in those centrin2-deficient and D77A cells that made cilia, the cilia were shorter than those seen in wild-type and rescued null cells, and the 4DA cells showed slightly longer cilia than controls (Figure 6A, B). To test the notion that centrin2 levels might affect tubulin stabilisation, we overexpressed centrin2 in wild-type and *CETN2* null cells and measured the length of cilia observed after 18h serum starvation. We found that cilia were significantly longer in the cells where centrin2 was expressed in addition to the endogenous amount (Figure 6C, D). These findings support a role for centrin2 in controlling the extension and stabilisation of the axoneme.

A number of centrin functions have been ascribed to its assembly of multimeric structures, including self-aggregation (Wiech et al., 1996, Azimzadeh et al., 2009, Kilmartin, 2003, Martinez-Sanz et al., 2006). The accessibility of the binding regions on centrin2 to interacting peptide sequences depends on structural shifts induced by calcium binding, with different calcium-dependent effects seen in different species (reviewed in (Dantas et al., 2012, Zhang and He, 2011)). To explore how centrin interactions are affected by the calcium-binding capacity of the EF-hands, we performed immunoprecipitation experiments with centrin2 and the 4DA mutant form. As shown in Figure 7, centrin2 co-immunoprecipitated with both SFI1 and POC5 from hTERT-RPE1 cells, although with a diminishing amount of both following serum starvation. These interactions required centrin2 and were dependent on its EF-hands, although a potential caveat lies in the reduced level of the 4DA form of centrin2 that we precipitated in this experiment, similar to those results seen with the XPC interaction. These observations show that a marked defect in centrin2-containing complex assembly results from the loss of EF-hand functioning, which is consistent with a model in which centrin2 multimerisation contributes to primary ciliogenesis.

Discussion

Here we examined the requirement for the EF-hands of human centrin2 in primary ciliogenesis and nucleotide excision repair and found a distinct separation of the functional requirements for these two activities of the protein. While mutagenesis of individual EF-hands still allowed the centrosome localisation of centrin2, we saw a marked impact on ciliogenesis when even a single EF-hand was disrupted, with problems with axonemal extension or stabilisation, localization of TTBK2 to apparently intact distal appendages, removal of CP110 and centriolar satellite dynamics. These defects were independent of the localisation of centrin2 to the

centriolar distal lumen, as we observed them in individual EF-hand mutants that localised to centrioles, as well as in the 4DA mutant, which did not. Nevertheless, in vitro NER activity was intact even in experiments that used only the 4DA mutant form of centrin2, in which all 4 EF-hands had been mutated. Furthermore, clonogenic survival after UV irradiation was normal in cells that expressed the 4DA mutant. We observed an analogous result in chicken DT40 cells, where the 4DA mutant was also defective in centriole localisation but was capable of allowing wild-type levels of survival after UV irradiation in a clonogenic survival assay (Dantas et al., 2013). The contrasting phenotypic data with respect to these two functions of centrin2 suggest that each of the EF-hands specifies a key activity of centrin2 in ciliogenesis or that the structural changes imposed by mutation of any of the EF-hands abrogate a centrosomal or ciliary function of human centrin2 that is dispensable in NER.

A model for centrin function is that calcium binding allows the protein to interact with target peptides, with calcium mediating a switch to a higher-affinity state of the protein for specific binding partners, as in the case of *Chlamydomonas* centrin and a Kar1 peptide (Veeraraghavan et al., 2002, Ortiz et al., 2005, Hu et al., 2004) or yeast Cdc31p and a Kar1p peptide (Geier et al., 1996). Work with *Scherffelia dubia* centrin and human peptides found that low-affinity N-terminal peptide binding sites became activated in the presence of calcium (Radu et al., 2010), although the extent to which the XPC peptide binding in that study is relevant may be questionable, given our findings on the NER capacity of the 4DA mutant. In vitro data have indicated that the high-affinity calcium-binding sites of human centrin1 and centrin2 lie in the C-terminal EF-hand domains, with the N-terminal EF-hands being of lower affinity and responding to the calcium occupancy status of the C-terminal sites (Durussel et al., 2000, Matei et al., 2003, Yang et al., 2006, Nishi et al., 2013). Interestingly, analysis of the crystal structure of the homologous mouse centrin1 protein suggested that calcium occupancy of the N-terminal EF-hands facilitates centrin1 dimerization through structural alterations that occur upon

binding of each of the four EF-hands (Kim et al., 2017). While these observations imply that a hierarchy of calcium affinities determines the roles of the individual EF-hands in centrin functions, we observed relatively little phenotypic distinction between the individual EF-hand mutants, the 4DA mutant and the centrin2 nulls in terms of ciliation. Unexpectedly, we saw a marked impact of the D77A mutation, one of the N-terminal EF-hands. However, the D41,77A double mutant showed a less dramatic phenotype and so it is unclear how this specific mutant impacts on centrin2 activities.

Previous analyses have demonstrated that centrin forms large aggregates, with both itself and its interactors, such as XPC (Araki et al., 2001), Kar1p (Spang et al., 1995), Sfi1p (Kilmartin, 2003) and CP110 (Tsang et al., 2006). Several studies have demonstrated the importance of calcium binding in self-aggregation of centrins from multiple species (Wiech et al., 1996, Tourbez et al., 2004, Yang et al., 2006, Li et al., 2006, Wang et al., 2018), as well as in the assembly of multimeric complexes with Sfi1p (Kilmartin, 2003, Li et al., 2006, Martinez-Sanz et al., 2006). Our data clearly indicate the need for calcium binding capacity in allowing the assembly of human centrin2-SFI1-POC5 complexes, consistent with previous observations we made on the requirement for centrin in the assembly of POC5 aggregate structures (Dantas et al., 2013). POC5 is required for centriole elongation, although its role is not yet understood (Azimzadeh et al., 2009). Overexpressed POC5 can assemble into linear aggregates in a centrin-dependent manner (Dantas et al., 2013). SFI1p-Cdc31p filament assembly is necessary for spindle pole duplication in budding yeast, potentially providing a scaffold for extension of the half-bridge (Li et al., 2006). While control of SFI1-centrin filament dynamics through calcium-regulated changes in centrin conformation was proposed as a contractility mechanism (Kilmartin, 2003) and demonstrated by analysis of the infraciliary lattice contractility in *Paramecium tetraurelia* (Gogendeau et al., 2007), it is not clear how this affects the extension of the primary cilium in human cells. In vitro analyses of the impact calcium chelation on the

assembly of this complex showed little effect with the yeast proteins, but a reduction with the human centrin2 protein was reported (Kilmartin, 2003). Together, these data indicate that SFI1 and POC5 are assembled into larger complexes that involve centrin2, although the phenotypic impact of the loss of such complexes in the absence of functional centrin2 remains to be defined.

We also noted that centrin2 loss or calcium-binding deficiency impacted on centriolar satellite aggregation, as measured by PCM1 signal. Centriolar satellites have been suggested to act as regulators of centrosome duplication by controlling availability of centrosome components (Dammermann and Merdes, 2002, Kubo and Tsukita, 2003, Firat-Karalar et al., 2014, Tollenaere et al., 2015) and recent data have similarly implicated them in ciliogenesis (Odabasi et al., 2019, Quarantotti et al., 2019). The reduction of ciliogenesis in centrin2-deficient or EF-hand mutant-expressing cells may thus reflect deficient aggregation of centrosome regulators in centriolar satellites.

An alternative explanation for the defects in ciliogenesis that we observed here is instability in axonemal tubulin structures in the absence of centrin or its EF-hands. Such an idea would be consistent with the reduced ciliation frequency and length, as determined by measurement with tubulin markers, and the more limited impact seen when ARL13B was used as a marker. In support of this notion are the basal body stability defects that were described in *Tetrahymena* upon deletion or mutagenesis of the C-terminal EF-hands of Cen1, the principal centrin2 orthologue in that organism (Stemm-Wolf et al., 2005, Vonderfecht et al., 2011). This model suggests that centrin contributes to ciliogenesis by regulating dynamic protein assemblies at the distal end of the centrioles. However, the mechanism by which centrin can affect tubulin assembly in ciliogenesis is unclear. A proteomic study of the interactions of centriolar proteins did not describe centrin as a tubulin interactor (Gupta et al., 2015), so that such regulation may be indirect. Given the effects that centrin deficiency or EF-hand mutagenesis have on key

aggregate structures, CP110 is an attractive candidate for mediating centrin functions in ciliogenesis. CP110 is a negative regulator of centriole length and its depletion facilitates microtubule extension, although additional activities are necessary for ciliogenesis proper (Schmidt et al., 2009, Spektor et al., 2007). CP110 can be co-immunoprecipitated with centrin and co-fractionates with it in large (>MDa) complexes (Tsang et al., 2006). Its centrin2-dependent removal from the distal end of the centriole is necessary for primary ciliogenesis (Prosser and Morrison, 2015). As TTBK2 localisation is also required for the correctly-regulated removal of CP110 (Cajanek and Nigg, 2014, Oda et al., 2014), CP110 dynamics may be controlled by centrin through interactions in larger complexes, potentially in centriolar satellites (Tsang and Dynlacht, 2013), or through TTBK2 regulation at the distal end of the centriole. An outstanding question is whether POC5 and SFI1 play a role in these processes. The availability of NER-competent, ciliation-defective centrin2 mutants will allow the dissection of the interactions of centrin in these activities.

Materials and Methods

Cell culture

hTERT-RPE1 cells were obtained from ATCC and grown in DMEM-F12 medium with 10% fetal bovine serum and 1% penicillin-streptomycin in a humidified 5% CO^2 atmosphere at 37°C. *CETN2* knockout clones were generated in a previous study (Prosser and Morrison, 2015). Mycoplasma testing was performed every 2 months. Transfections were performed using Lipofectamine 2000 (Thermo Fisher) as per the manufacturers' instructions. For stable transfections, cells were trypsinised 18h post-transfection and serial dilutions were performed into medium containing 1 mg/ml G418 (Invitrogen, CA, USA). Cells were placed under selection for 7-14 days, after which colonies were lifted using cloning discs (Sigma-Aldrich).

Serum starvation conditions consisted of DMEM-F12 medium with 0.1% FBS. SAG (EMD Millipore) was used on cells at 100 nM which was prepared from a 1M stock made up in DMSO. Irradiations were performed using a ^{137}Cs source at 9.5 Gy/ minute (Mainance Engineering) or with an NU-6 254 nm UV-C lamp at 23 J/m^2/min (Benda). UV clonogenic survival assays were performed as previously described (Daly et al., 2016).

Cloning and molecular biology

Human *CETN2* cDNA sequence (Inanc et al., 2010) was cloned into pCMV-3tag-Myc (Agilent). Site-directed mutagenesis was performed using a Quick-Change II XL kit (Agilent) following the manufacturer's instructions with the following primer pairs: Centrin2 D41A (forward): 5'-CCGGGAAGCTTTTGATCTTTTCGCTGCGGATGGAACTGGCACCATAGATG-3'; (reverse): 5'-CATCTATGGTGCCAGTTCCATCCGCAGCGAAAAGATCAAAAGCTTCCCGG-3'; Centrin2 D77A (forward): 5'-TAAGAAAATGATAAGTGAAATTGCTAAGGAAGGGACAGGAAAAATGAA-3'; (reverse): 5'-TTCATTTTTCCTGTCCCTTCCTTAGCAATTTCACTTATCATTTTCTTA-3'; Centrin2 D114A (forward): 5'-AATCCTGAAAGCTTTCAAGCTCTTTGCTGATGATGAAACTGGGAAGATT-3'; (reverse) 5'-AATCTTCCCAGTTTCATCATCAGCAAAGAGCTTGAAAGCTTTCAGGATT-3'; Centrin2 D150A (forward): 5'-CTGCAGGAAATGATTGATGAAGCTGCTCGAGATGGAGATGGAGAGGTC-3'; (reverse): 5'-GACCTCTCCATCTCCATCTCGAGCAGCTTCATCAATCATTTCCTGCAG-3'. Each

single mutant was generated and additional rounds of mutagenesis performed subsequent to DNA sequence verification of the individual mutation (Source Biosciences). For bacterial expression, centrin2-encoding sequences were subcloned into the BamHI-XhoI sites of pGEX-4T (GE Healthcare). For RT-PCR, cDNA synthesis was performed using a High-Capacity RNA to cDNA kit (Agilent) and PCR using KOD Hot Start (Applied Biosystems), according to the manufacturers' instructions.

Immunoblotting

Whole-cell extracts were prepared with radioimmunoprecipitation assay buffer (50 mM Tris-HCl, pH 7.4, 1% NP-40, 0.25% sodium deoxycholate, 150 mM NaCl, 1 mM EDTA, with protease and phosphatase inhibitor cocktails). Blots were detected by ECL (GE Healthcare). The following primary antibodies were used: rabbit polyclonals against Centrin2 (15877-1-AP, Proteintech, 1:1000), phospho-CDK2 T160 (2561, Cell Signaling, 1:500), POC5 (A303-340A, Bethyl, 1:500), SFI1 (13550-1-AP, Proteintech, 1:400); rabbit monoclonals against GAPDH (14C10, Cell Signalling, 1:5000), phospho-CHK1 S345 (133D3, Cell Signalling, 1:1000) and mouse monoclonals against CDK2 (D12, Santa Cruz, 1:1000), CHK1 (DCS310, Sigma, 1:500). HRP-conjugated goat anti-mouse or anti-rabbit secondary antibodies were used at 1:5000 (Jackson ImmunoResearch Laboratories).

Immunoprecipitation

Whole cell extracts were prepared in IP lysis buffer (50 mM Tris HCl, pH 7.4; 150mM NaCl; 1mM EDTA pH 8.0; 20% Glycerol; 0.5% sodium deoxycholate and 1% IGEPAL CA-630) with protease inhibitor cocktail and 1:1000 dilution of benzonase (Sigma-Aldrich) added fresh before use. Samples were incubated with rotation for 60 minutes at 4°C, then centrifuged for 20 min at 13,200 *g* at 4°C. Supernatants were transferred to fresh Eppendorf tubes. Protein A/G beads (Santa Cruz) were washed 3 times with IP lysis buffer, then incubated with primary

antibody for 2 h at 4°C. Bead-antibody complexes were washed 3 times with IP lysis buffer and incubated with 1-2 mg total cell extracts overnight at 4°C on a rotating wheel. Beads were then spun down at 250 *g* for 5 minutes and the supernatant discarded, after which the bead-bound proteins were washed 5 times in IP lysis buffer prior to boiling in sample buffer.

Expression of recombinant proteins in *E. coli*

Glutathione S-transferase (GST) fusion proteins were expressed in *E. coli* BL21-CodonPlus-RIL by induction with 1 mM IPTG for 3 h. Cell pellets were resuspended in TEN buffer (10 mM Tris-Cl, pH 8.0; 1 mM EDTA; 100 mM NaCl) supplemented with protease inhibitors, and then disrupted by sonication. The lysates were centrifuged for 30 min at 200,000 *g* at 2°C. The clarified extracts were loaded onto a GSTrap HP column (GE Healthcare) equilibrated with TEN-T buffer (TEN buffer containing 0.1% Triton X-100). After extensive washing with TEN-T buffer, bound proteins were eluted using GST elution buffer (20 mM Tris-HCl, pH 8.4; 0.1 M NaCl; 0.1% Triron X-100; 20 mM glutathione). Eluates were dialyzed against buffer containing 50 mM Tris-HCl, pH 8.0, and 10 mM $CaCl_2$, added to washed Thrombin CleanCleave beads (Sigma-Aldrich), and rotated overnight at room temperature. After removal of the beads by passing through disposable plastic columns (Thermo Fisher), the samples were loaded onto a RESOURCE Q column (GE Healthcare), which was tandemly connected to a GSTrap HP pre-column and equilibrated with buffer Q (50 mM Tris-HCl, pH 8.0; 1 mM DTT). After extensive washing with buffer Q, the pre-column was disconnected and proteins bound to the RESOURCE Q column was eluted with a linear NaCl gradient (0-0.5 M) in buffer Q. Finally, the peak fractions were further purified with size exclusion chromatography with a Superdex 75 column (GE Healthcare) equilibrated with 1 x PBS.

In vitro protein interaction and NER assays

Anti-FLAG Magnetic beads (Wako) were washed thrice in XPC dilution buffer (20 mM Na-phosphate, pH 7.8; 10% glycerol; 1 mM EDTA; 0.3 M NaCl; 1 mM DTT) then incubated in 100 µl of the same buffer containing 200 ng of FLAG-XPC-RAD23B-His complex and 20 µg of acetylated BSA for 2 h at 4˚C with stirring. The beads were then washed thrice with XPC dilution buffer and and incubated with 300 ng of GST-centrin2 in 100 µl of XPC dilution buffer containing 20 µg of acetylated BSA, for 2h at 4˚C with stirring. The beads were then washed nine times with XPC dilution buffer. Bound complexes were competed off by the addition of 40 µl of 0.5 mg/ml of FLAG peptide, which was stirred at 4°C for 3 h before the beads were removed by magnet and the samples prepared for polyacrylamide gel electrophoresis.

In vitro NER dual incision assays were carried out with purified NER proteins and internally ^{32}P-labeled DNA substrate with or without a single 6-4 PP as previously described (Nishi et al., 2005, Nishi et al., 2013). The XPC-RAD23B complex (10 ng) was mixed with 10 ng of centrin2 (WT or 4DA) and pre-incubated at 4°C for 30 min before being added to the standard reaction mixture. After incubation at 30°C for various time periods, DNA samples were purified and subjected to denaturing polyacrylamide gel electrophoresis. Dried gels were exposed to BAS imaging plates (Fujifilm) and analyzed with Typhoon FLA 9500 scanner and ImageQuant TL software (GE Healthcare).

Microscopy

hTERT-RPE1 cells were grown on sterile glass coverslips and fixed in methanol/5 mM EGTA at -20°C for 10 min. For microscopy after staining with acetylated or detyrosinated tubulin, cells were incubated on ice for 35 minutes to depolymerise the microtubule cytoskeleton before

fixation. Cells were blocked in 1% BSA, before 1 h incubation with primary antibodies and 45 min incubation with Alexa 488- or 594-labelled donkey secondary antibodies (Invitrogen). Mouse monoclonal antibodies used were as follows: acetylated tubulin (6-11B-1, Sigma, 1:1000), γ-tubulin (GTU88, Sigma, 1:200), Centrin2 (20H5, Millipore, 1:1000), Centrin3 (3E6, Abnova, 1:1000), CEP164 (1F3G10, (Daly et al., 2016), 1:10000), polyglutamylated tubulin (GT335, Adipogen, 1:500). Rabbit polyclonal antibodies used were against Arl13b (17711-1-AP, Proteintech, 1:1000), Centrin2 (15877-1-AP, Proteintech, 1:1000), CEP135 (Ab75005, Abcam, 1:500), CEP164 (HPA037606, Sigma, 1:1000), CP110 (12780-1-AP, Proteintech, 1:1000), Smoothened (ab38686, Abcam, 1:500), TTBK2 (15072-1-AP, Proteintech, 1:500). Goat polyclonal Sc-50164 (Santa Cruz) was used at 1:400. DNA was stained with Hoechst 33258 (Sigma-Aldrich). Coverslips were mounted in 80% v/v glycerol in PBS containing 3% w/v N-propyl-gallate and DAPI.

Fluorescence imaging and counts were performed using an Olympus BX51 microscope (with a Hamamatsu C10600 camera) or IX81 microscope (Hamamatsu C4742-80-12AG camera), using a 100x oil (NA 1.35) objective. Serial z-sections were taken, merged and saved as Photoshop version CS4 (Adobe Systems). Merges and individual channel images were exported as TIFFs for publication. Volocity analysis software v6.2.1 (Perkin-Elmer) was used for signal intensity measurements, in which deconvolved maximum intensity projections collapsed the 3D volumes into 2D images for determination of fluorescence intensity within a 25μm^2 circle around each centriole.

dSTORM imaging was performed as previously described in detail (Yang et al., 2018). Briefly, rat polyclonal anti-SCLT1 (1:250, (Tanos et al., 2013)), rabbit anti-CEP164 (45330002, Novus Biologicals, 1:2000), and rabbit anti-TTBK2 (15072-1-AP, Proteintech, 1:500) were used as primary antibodies. Alexa Fluor 647 (anti-rabbit A21245, Thermo Fisher) and Cy3B-

conjugated secondary antibody (1:100, (Yang et al., 2018)) were used as secondary antibodies. Imaging was performed with an Evolve 512 Delta EMCCD camera (Photometrics), a 637 nm laser (OBIS 637 LX 140 mW, Coherent), a 561 nm laser (Jive 561 150 mW, Cobolt), and a 405 nm laser (OBIS 405 LX 100 mW, Coherent), connecting to a modified inverted microscope (Eclipse Ti-E, Nikon) using a 100Å~ 1.49 numerical aperture oil-immersion objective (CFI Apo TIRF, Nikon). Image analysis was performed with the MetaMorph Super-resolution module (Molecular Devices).

Statistical analysis

Statistical analyses were performed with Prism v5.0 (GraphPad).

Competing interests

No competing interests declared.

Author contributions

Conceptualization, C.G.M. Investigation: E.K., H.T., W.M.C. Data analysis: E.K., H.T., W.M.C., J.-C.L., K.S., C.G.M. Writing (original draft): C.G.M. Writing (review and editing): E.K., W.M.C., J.-C.L., K.S. Supervision, administration, funding acquisition: C.G.M., J.-C.L., K.S.

Funding

This work was funded by Science Foundation Ireland International Strategic Cooperation Award 13/ISCA/2846 and European Commission SEC-2009-4.3-02, project 242361 'BOOSTER'. E.M.K. received a King Abdullah Foreign Scholarship from the Saudi Arabian Ministry of Higher Education. S.L.P. was the recipient of a European Union Horizon 2020 Marie Skłodowska-Curie Global Fellowship (No. 702601). W.M.C. was supported by Academia Sinica, Taiwan grant AS-CDA-104-M06. J.-C.L. was supported by the Ministry of Science and Technology, Taiwan grant 107-2313-B-001-009. This work was supported by Japan Society for the Promotion of Science KAKENHI grant number JP16H06307 to K.S.

References

Acu, I. D., Liu, T., Suino-Powell, K., Mooney, S. M., D'assoro, A. B., Rowland, N., Muotri, A. R., Correa, R. G., Niu, Y., Kumar, R. & Salisbury, J. L. (2010). Coordination of centrosome homeostasis and DNA repair is intact in MCF-7 and disrupted in MDA-MB 231 breast cancer cells. *Cancer Res,* **70,** 3320-8.

Araki, M., Masutani, C., Takemura, M., Uchida, A., Sugasawa, K., Kondoh, J., Ohkuma, Y. & Hanaoka, F. (2001). Centrosome protein centrin 2/caltractin 1 is part of the xeroderma pigmentosum group C complex that initiates global genome nucleotide excision repair. *J Biol Chem,* **276,** 18665-72.

Azimzadeh, J., Hergert, P., Delouvee, A., Euteneuer, U., Formstecher, E., Khodjakov, A. & Bornens, M. (2009). hPOC5 is a centrin-binding protein required for assembly of full-length centrioles. *J Cell Biol,* **185,** 101-14.

Betzig, E., Patterson, G. H., Sougrat, R., Lindwasser, O. W., Olenych, S., Bonifacino, J. S., Davidson, M. W., Lippincott-Schwartz, J. & Hess, H. F. (2006). Imaging intracellular fluorescent proteins at nanometer resolution. *Science,* **313,** 1642-5.

Bourke, E., Brown, J. A., Takeda, S., Hochegger, H. & Morrison, C. G. (2010). DNA damage induces Chk1-dependent threonine-160 phosphorylation and activation of Cdk2. *Oncogene,* **29,** 616-24.

Braun, D. A. & Hildebrandt, F. (2017). Ciliopathies. *Cold Spring Harb Perspect Biol,* **9**.

Cajanek, L. & Nigg, E. A. (2014). Cep164 triggers ciliogenesis by recruiting Tau tubulin kinase 2 to the mother centriole. *Proc Natl Acad Sci U S A,* **111,** E2841-50.

Chen, Z., Indjeian, V. B., Mcmanus, M., Wang, L. & Dynlacht, B. D. (2002). CP110, a cell cycle-dependent CDK substrate, regulates centrosome duplication in human cells. *Dev Cell,* **3,** 339-50.

D'angiolella, V., Donato, V., Vijayakumar, S., Saraf, A., Florens, L., Washburn, M. P., Dynlacht, B. & Pagano, M. (2010). SCF(Cyclin F) controls centrosome homeostasis and mitotic fidelity through CP110 degradation. *Nature,* **466,** 138-42.

Daly, O. M., Gaboriau, D., Karakaya, K., King, S., Dantas, T. J., Lalor, P., Dockery, P., Kramer, A. & Morrison, C. G. (2016). Gene-targeted CEP164-deficient cells show a ciliation defect with intact DNA repair capacity. *J Cell Sci,* **129,** 1769-74.

Dammermann, A. & Merdes, A. (2002). Assembly of centrosomal proteins and microtubule organization depends on PCM-1. *J Cell Biol,* **159,** 255-66.

Dantas, T. J., Daly, O. M., Conroy, P. C., Tomas, M., Wang, Y., Lalor, P., Dockery, P., Ferrando-May, E. & Morrison, C. G. (2013). Calcium-binding capacity of centrin2 is required for linear POC5 assembly but not for nucleotide excision repair. *PLoS One,* **8,** e68487.

Dantas, T. J., Daly, O. M. & Morrison, C. G. (2012). Such small hands: the roles of centrins/caltractins in the centriole and in genome maintenance. *Cell Mol Life Sci,* **69,** 2979-97.

Dantas, T. J., Wang, Y., Lalor, P., Dockery, P. & Morrison, C. G. (2011). Defective nucleotide excision repair with normal centrosome structures and functions in the absence of all vertebrate centrins. *J Cell Biol,* **193,** 307-18.

Durussel, I., Blouquit, Y., Middendorp, S., Craescu, C. T. & Cox, J. A. (2000). Cation- and peptide-binding properties of human centrin 2. *FEBS Lett,* **472,** 208-12.

Firat-Karalar, E. N., Rauniyar, N., Yates, J. R., 3rd & Stearns, T. (2014). Proximity interactions among centrosome components identify regulators of centriole duplication. *Curr Biol,* **24,** 664-70.

Flanagan, A. M., Stavenschi, E., Basavaraju, S., Gaboriau, D., Hoey, D. A. & Morrison, C. G. (2017). Centriole splitting caused by loss of the centrosomal linker protein C-

NAP1 reduces centriolar satellite density and impedes centrosome amplification. *Mol Biol Cell,* **28,** 736-745.

Geier, B. M., Wiech, H. & Schiebel, E. (1996). Binding of centrins and yeast calmodulin to synthetic peptides corresponding to binding sites in the spindle pole body components Kar1p and Spc110p. *J Biol Chem,* **271,** 28366-74.

Geiser, J. R., Van Tuinen, D., Brockerhoff, S. E., Neff, M. M. & Davis, T. N. (1991). Can calmodulin function without binding calcium? *Cell,* **65,** 949-59.

Gifford, J. L., Walsh, M. P. & Vogel, H. J. (2007). Structures and metal-ion-binding properties of the Ca2+-binding helix-loop-helix EF-hand motifs. *Biochem J,* **405,** 199-221.

Goetz, S. C. & Anderson, K. V. (2010). The primary cilium: a signalling centre during vertebrate development. *Nat Rev Genet,* **11,** 331-44.

Goetz, S. C., Liem, K. F., Jr. & Anderson, K. V. (2012). The spinocerebellar ataxia-associated gene Tau tubulin kinase 2 controls the initiation of ciliogenesis. *Cell,* **151,** 847-58.

Gogendeau, D., Beisson, J., De Loubresse, N. G., Le Caer, J. P., Ruiz, F., Cohen, J., Sperling, L., Koll, F. & Klotz, C. (2007). An Sfi1p-like centrin-binding protein mediates centrin-based Ca2+ -dependent contractility in Paramecium tetraurelia. *Eukaryot Cell,* **6,** 1992-2000.

Graser, S., Stierhof, Y. D., Lavoie, S. B., Gassner, O. S., Lamla, S., Le Clech, M. & Nigg, E. A. (2007). Cep164, a novel centriole appendage protein required for primary cilium formation. *J Cell Biol,* **179,** 321-30.

Gupta, G. D., Coyaud, E., Goncalves, J., Mojarad, B. A., Liu, Y., Wu, Q., Gheiratmand, L., Comartin, D., Tkach, J. M., Cheung, S. W., Bashkurov, M., Hasegan, M., Knight, J. D., Lin, Z. Y., Schueler, M., Hildebrandt, F., Moffat, J., Gingras, A. C.,

Raught, B. & Pelletier, L. (2015). A Dynamic Protein Interaction Landscape of the Human Centrosome-Cilium Interface. *Cell,* **163,** 1484-99.

Heilemann, M., Van De Linde, S., Schuttpelz, M., Kasper, R., Seefeldt, B., Mukherjee, A., Tinnefeld, P. & Sauer, M. (2008). Subdiffraction-resolution fluorescence imaging with conventional fluorescent probes. *Angew Chem Int Ed Engl,* **47,** 6172-6.

Hu, H., Sheehan, J. H. & Chazin, W. J. (2004). The mode of action of centrin. Binding of Ca2+ and a peptide fragment of Kar1p to the C-terminal domain. *J Biol Chem,* **279,** 50895-903.

Inanc, B., Dodson, H. & Morrison, C. G. (2010). A centrosome-autonomous signal that involves centriole disengagement permits centrosome duplication in G2 phase after DNA damage. *Mol Biol Cell,* **21,** 3866-77.

Kilmartin, J. V. (2003). Sfi1p has conserved centrin-binding sites and an essential function in budding yeast spindle pole body duplication. *J Cell Biol,* **162,** 1211-21.

Kim, S. Y., Kim, D. S., Hong, J. E. & Park, J. H. (2017). Crystal Structure of Wild-Type Centrin 1 from Mus musculus Occupied by Ca2. *Biochemistry (Mosc),* **82,** 1129-1139.

Kleylein-Sohn, J., Westendorf, J., Le Clech, M., Habedanck, R., Stierhof, Y. D. & Nigg, E. A. (2007). Plk4-induced centriole biogenesis in human cells. *Dev Cell,* **13,** 190-202.

Kobayashi, T., Kim, S., Lin, Y. C., Inoue, T. & Dynlacht, B. D. (2014). The CP110-interacting proteins Talpid3 and Cep290 play overlapping and distinct roles in cilia assembly. *J Cell Biol,* **204,** 215-29.

Kodani, A., Yu, T. W., Johnson, J. R., Jayaraman, D., Johnson, T. L., Al-Gazali, L., Sztriha, L., Partlow, J. N., Kim, H., Krup, A. L., Dammermann, A., Krogan, N., Walsh, C. A. & Reiter, J. F. (2015). Centriolar satellites assemble centrosomal microcephaly proteins to recruit CDK2 and promote centriole duplication. *Elife,* **4**.

Kubo, A. & Tsukita, S. (2003). Non-membranous granular organelle consisting of PCM-1: subcellular distribution and cell-cycle-dependent assembly/disassembly. *J Cell Sci,* **116,** 919-28.

Li, J., D'angiolella, V., Seeley, E. S., Kim, S., Kobayashi, T., Fu, W., Campos, E. I., Pagano, M. & Dynlacht, B. D. (2013). USP33 regulates centrosome biogenesis via deubiquitination of the centriolar protein CP110. *Nature,* **495,** 255-9.

Li, S., Sandercock, A. M., Conduit, P., Robinson, C. V., Williams, R. L. & Kilmartin, J. V. (2006). Structural role of Sfi1p-centrin filaments in budding yeast spindle pole body duplication. *J Cell Biol,* **173,** 867-77.

Loffler, H., Fechter, A., Liu, F. Y., Poppelreuther, S. & Kramer, A. (2013). DNA damage-induced centrosome amplification occurs via excessive formation of centriolar satellites. *Oncogene,* **32,** 2963-72.

Martinez-Sanz, J., Yang, A., Blouquit, Y., Duchambon, P., Assairi, L. & Craescu, C. T. (2006). Binding of human centrin 2 to the centrosomal protein hSfi1. *Febs J,* **273,** 4504-15.

Matei, E., Miron, S., Blouquit, Y., Duchambon, P., Durussel, I., Cox, J. A. & Craescu, C. T. (2003). C-terminal half of human centrin 2 behaves like a regulatory EF-hand domain. *Biochemistry,* **42,** 1439-50.

Middendorp, S., Kuntziger, T., Abraham, Y., Holmes, S., Bordes, N., Paintrand, M., Paoletti, A. & Bornens, M. (2000). A role for centrin 3 in centrosome reproduction. *J Cell Biol,* **148,** 405-16.

Mikule, K., Delaval, B., Kaldis, P., Jurcyzk, A., Hergert, P. & Doxsey, S. (2007). Loss of centrosome integrity induces p38-p53-p21-dependent G1-S arrest. *Nat Cell Biol,* **9,** 160-70.

Nishi, R., Okuda, Y., Watanabe, E., Mori, T., Iwai, S., Masutani, C., Sugasawa, K. & Hanaoka, F. (2005). Centrin 2 stimulates nucleotide excision repair by interacting with xeroderma pigmentosum group C protein. *Mol Cell Biol,* **25,** 5664-74.

Nishi, R., Sakai, W., Tone, D., Hanaoka, F. & Sugasawa, K. (2013). Structure-function analysis of the EF-hand protein centrin-2 for its intracellular localization and nucleotide excision repair. *Nucleic Acids Res,* **41,** 6917-29.

Oda, T., Chiba, S., Nagai, T. & Mizuno, K. (2014). Binding to Cep164, but not EB1, is essential for centriolar localization of TTBK2 and its function in ciliogenesis. *Genes Cells,* **19,** 927-40.

Odabasi, E., Gul, S., Kavakli, I. H. & Firat-Karalar, E. N. (2019). Centriolar satellites are required for efficient ciliogenesis and ciliary content regulation. *EMBO Rep*., in press.

Ogungbenro, Y. A., Tena, T. C., Gaboriau, D., Lalor, P., Dockery, P., Philipp, M. & Morrison, C. G. (2018). Centrobin controls primary ciliogenesis in vertebrates. *J Cell Biol,* **217,** 1205-1215.

Ohta, T., Essner, R., Ryu, J. H., Palazzo, R. E., Uetake, Y. & Kuriyama, R. (2002). Characterization of Cep135, a novel coiled-coil centrosomal protein involved in microtubule organization in mammalian cells. *J Cell Biol,* **156,** 87-99.

Ortiz, M., Sanoguet, Z., Hu, H., Chazin, W. J., Mcmurray, C. T., Salisbury, J. L. & Pastrana-Rios, B. (2005). Dynamics of hydrogen-deuterium exchange in Chlamydomonas centrin. *Biochemistry,* **44,** 2409-18.

Paoletti, A., Moudjou, M., Paintrand, M., Salisbury, J. L. & Bornens, M. (1996). Most of centrin in animal cells is not centrosome-associated and centrosomal centrin is confined to the distal lumen of centrioles. *J Cell Sci,* **109 (Pt 13),** 3089-102.

Prosser, S. L. & Morrison, C. G. (2015). Centrin2 regulates CP110 removal in primary cilium formation. *J Cell Biol,* **208,** 693-701.

Prosser, S. L., Straatman, K. R. & Fry, A. M. (2009). Molecular dissection of the centrosome overduplication pathway in S-phase-arrested cells. *Mol Cell Biol,* **29,** 1760-73.

Quarantotti, V., Chen, J. X., Tischer, J., Gonzalez Tejedo, C., Papachristou, E. K., D'santos, C. S., Kilmartin, J. V., Miller, M. L. & Gergely, F. (2019). Centriolar satellites are acentriolar assemblies of centrosomal proteins. *EMBO J.*, in press.

Radu, L., Durussel, I., Assairi, L., Blouquit, Y., Miron, S., Cox, J. A. & Craescu, C. T. (2010). Scherffelia dubia centrin exhibits a specific mechanism for Ca(2+)-controlled target binding. *Biochemistry,* **49,** 4383-94.

Rust, M. J., Bates, M. & Zhuang, X. (2006). Sub-diffraction-limit imaging by stochastic optical reconstruction microscopy (STORM). *Nat Methods,* **3,** 793-5.

Salisbury, J. L., Suino, K. M., Busby, R. & Springett, M. (2002). Centrin-2 is required for centriole duplication in mammalian cells. *Curr Biol,* **12,** 1287-92.

Sanchez, I. & Dynlacht, B. D. (2016). Cilium assembly and disassembly. *Nat Cell Biol,* **18,** 711-7.

Schmidt, T. I., Kleylein-Sohn, J., Westendorf, J., Le Clech, M., Lavoie, S. B., Stierhof, Y. D. & Nigg, E. A. (2009). Control of centriole length by CPAP and CP110. *Curr Biol,* **19,** 1005-11.

Sorokin, S. (1962). Centrioles and the formation of rudimentary cilia by fibroblasts and smooth muscle cells. *J Cell Biol,* **15,** 363-77.

Spang, A., Courtney, I., Grein, K., Matzner, M. & Schiebel, E. (1995). The Cdc31p-binding protein Kar1p is a component of the half bridge of the yeast spindle pole body. *J Cell Biol,* **128,** 863-77.

Spektor, A., Tsang, W. Y., Khoo, D. & Dynlacht, B. D. (2007). Cep97 and CP110 suppress a cilia assembly program. *Cell,* **130,** 678-90.

Stemm-Wolf, A. J., Morgan, G., Giddings, T. H., Jr., White, E. A., Marchione, R., Mcdonald, H. B. & Winey, M. (2005). Basal body duplication and maintenance require one member of the Tetrahymena thermophila centrin gene family. *Mol Biol Cell,* **16,** 3606-19.

Tang, C. J., Fu, R. H., Wu, K. S., Hsu, W. B. & Tang, T. K. (2009). CPAP is a cell-cycle regulated protein that controls centriole length. *Nat Cell Biol,* **11,** 825-31.

Tanos, B. E., Yang, H. J., Soni, R., Wang, W. J., Macaluso, F. P., Asara, J. M. & Tsou, M. F. (2013). Centriole distal appendages promote membrane docking, leading to cilia initiation. *Genes Dev,* **27,** 163-8.

Tollenaere, M. A., Mailand, N. & Bekker-Jensen, S. (2015). Centriolar satellites: key mediators of centrosome functions. *Cell Mol Life Sci,* **72,** 11-23.

Tourbez, M., Firanescu, C., Yang, A., Unipan, L., Duchambon, P., Blouquit, Y. & Craescu, C. T. (2004). Calcium-dependent self-assembly of human centrin 2. *J Biol Chem,* **279,** 47672-80.

Tsang, W. Y., Bossard, C., Khanna, H., Peranen, J., Swaroop, A., Malhotra, V. & Dynlacht, B. D. (2008). CP110 suppresses primary cilia formation through its interaction with CEP290, a protein deficient in human ciliary disease. *Dev Cell,* **15,** 187-97.

Tsang, W. Y. & Dynlacht, B. D. (2013). CP110 and its network of partners coordinately regulate cilia assembly. *Cilia,* **2,** 9.

Tsang, W. Y., Spektor, A., Luciano, D. J., Indjeian, V. B., Chen, Z., Salisbury, J. L., Sanchez, I. & Dynlacht, B. D. (2006). CP110 cooperates with two calcium-binding proteins to regulate cytokinesis and genome stability. *Mol Biol Cell,* **17,** 3423-34.

Veeraraghavan, S., Fagan, P. A., Hu, H., Lee, V., Harper, J. F., Huang, B. & Chazin, W. J. (2002). Structural independence of the two EF-hand domains of caltractin. *J Biol Chem,* **277,** 28564-71.

Vonderfecht, T., Stemm-Wolf, A. J., Hendershott, M., Giddings, T. H., Jr., Meehl, J. B. & Winey, M. (2011). The two domains of centrin have distinct basal body functions in Tetrahymena. *Mol Biol Cell,* **22,** 2221-34.

Wang, W., Zhao, Y., Wang, H. & Yang, B. (2018). Crystal structure of the trimeric N-terminal domain of ciliate Euplotes octocarinatus centrin binding with calcium ions. *Protein Sci,* **27,** 1102-1108.

Wiech, H., Geier, B. M., Paschke, T., Spang, A., Grein, K., Steinkotter, J., Melkonian, M. & Schiebel, E. (1996). Characterization of green alga, yeast, and human centrins. Specific subdomain features determine functional diversity. *J Biol Chem,* **271,** 22453-61.

Yadav, S. P., Sharma, N. K., Liu, C., Dong, L., Li, T. & Swaroop, A. (2016). Centrosomal protein CP110 controls maturation of the mother centriole during cilia biogenesis. *Development,* **143,** 1491-501.

Yang, A., Miron, S., Duchambon, P., Assairi, L., Blouquit, Y. & Craescu, C. T. (2006). The N-terminal domain of human centrin 2 has a closed structure, binds calcium with a very low affinity, and plays a role in the protein self-assembly. *Biochemistry,* **45,** 880-9.

Yang, T. T., Chong, W. M., Wang, W. J., Mazo, G., Tanos, B., Chen, Z., Tran, T. M. N., Chen, Y. D., Weng, R. R., Huang, C. E., Jane, W. N., Tsou, M. B. & Liao, J. C. (2018). Super-resolution architecture of mammalian centriole distal appendages reveals distinct blade and matrix functional components. *Nat Commun*, **9,** 2023.

Ying, G., Avasthi, P., Irwin, M., Gerstner, C. D., Frederick, J. M., Lucero, M. T. & Baehr, W. (2014). Centrin 2 is required for mouse olfactory ciliary trafficking and development of ependymal cilia planar polarity. *J Neurosci*, **34,** 6377-88.

Zhang, Y. & He, C. Y. (2011). Centrins in unicellular organisms: functional diversity and specialization. *Protoplasma*, **249,** 459-467.

Figures

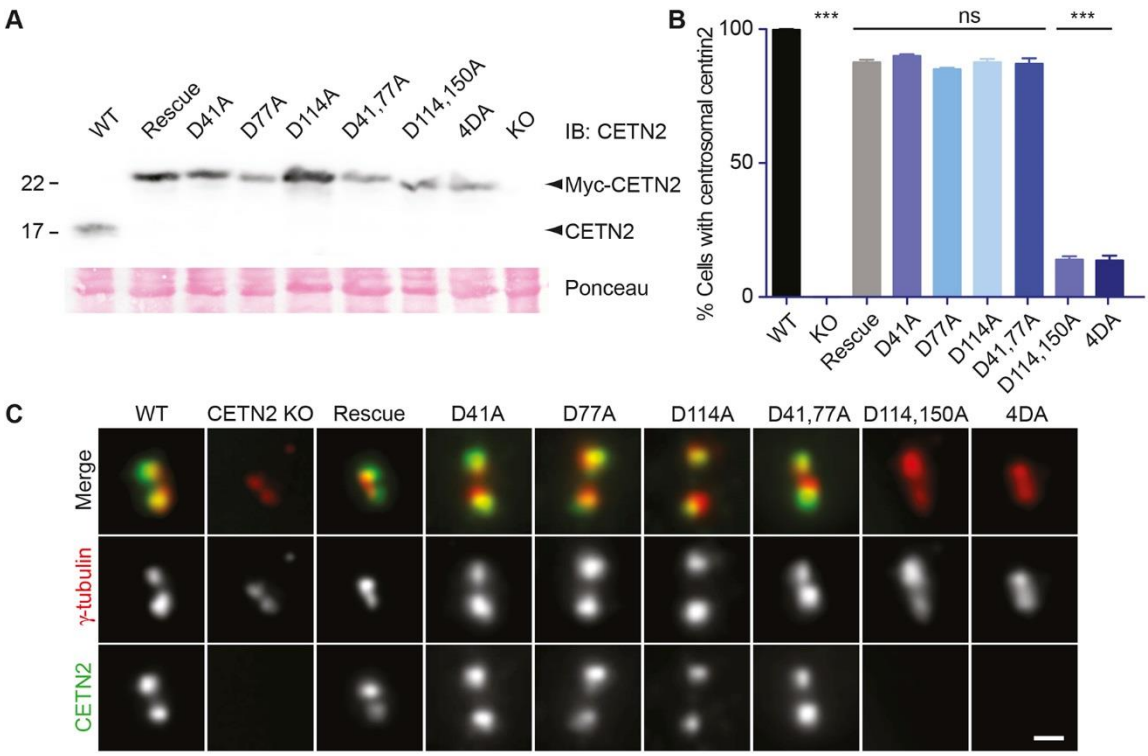

Figure 1 Centrin2 EF-hand mutants are deficient in centrosome localisation

A. Immunoblot showing the expression levels of endogenous centrin2 and the myc-centrin2 transgenes in the clones used here. Ponceau staining of the membrane was used as a loading control. WT, wild-type hTERT-RPE1 cells; KO, *CETN2* knockout; Rescue, *CETN2*$^{-/-}$ cells that express the wild-type form of centrin2. Size markers are indicated at left.

B. Bar graph shows the mean percentage ± s.e.m. of cells with centrosomal centrin2, as determined by co-staining for γ-tubulin, scored from 3 separate experiments in which at least 100 cells were counted. ***, $P<0.001$ compared to controls by ANOVA and Dunnett's multiple comparison test.

C. Immunofluorescence micrograph showing the localisation of wild-type and the indicated centrin2 mutants. Scale bar, 5 µm.

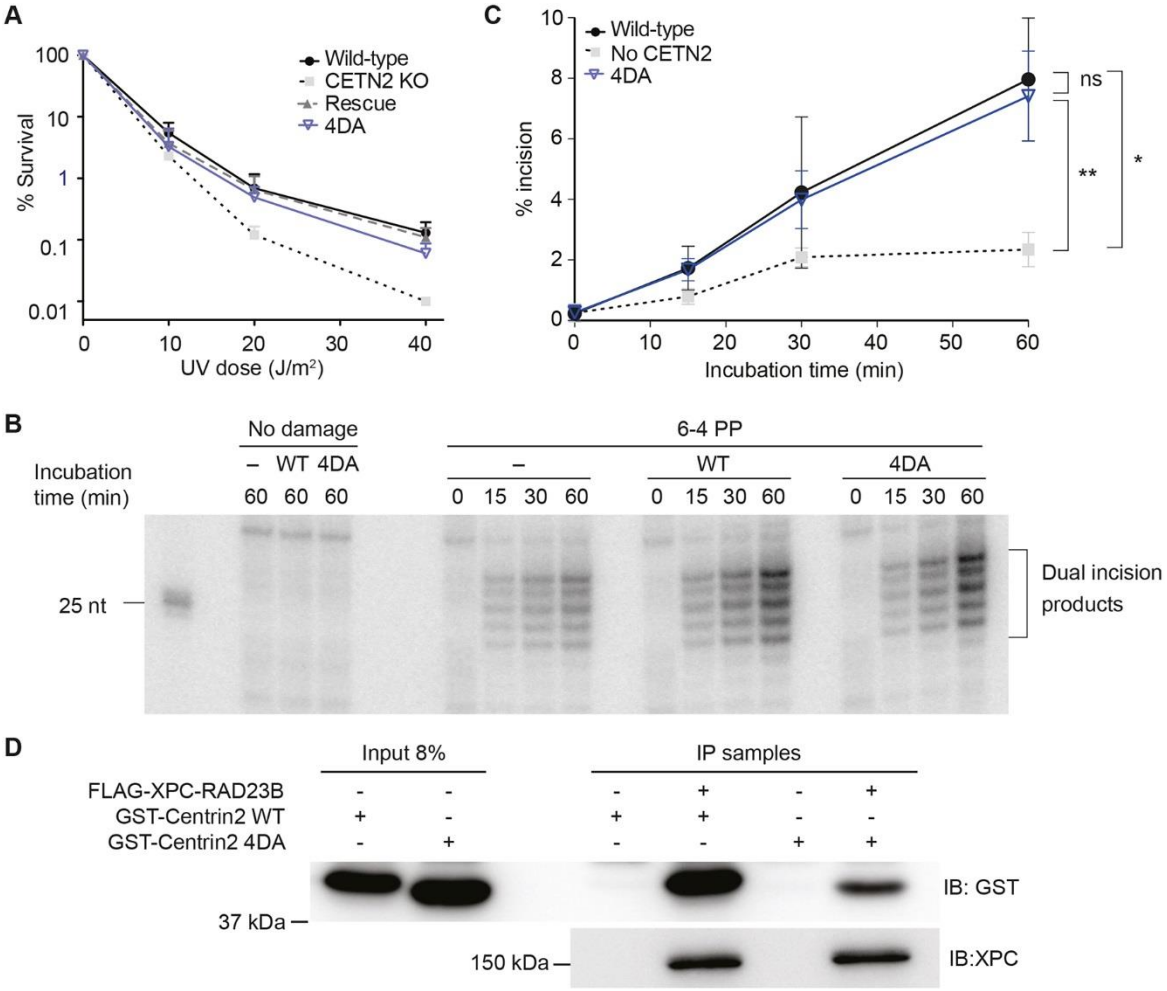

Figure 2 Centrin2 EF-hand mutants are proficient in NER

A. Clonogenic survival of cells of the indicated genotype after exposure to the indicated doses of UV irradiation. Datapoints represent the mean survival ± s.d. of 3 separate experiments.

B. In vitro NER dual incision assays with DNA containing a (6-4) photoproduct (6-4 PP) or undamaged control DNA in the presence of XPC-RAD23B complex and the indicated form of centrin2. -, no centrin2 control.

C. Quantitative analysis of the in vitro dual incision products. Mean values and standard deviations were calculated from three independent experiments. Statistical significance of the differences was evaluated with two-way ANOVA. *, $P<0.05$, **, $P<0.01$.

D. In vitro binding experiment showing the binding of purified, recombinant XPC-RAD23B complex to recombinant wild-type and 4DA centrin2 proteins.

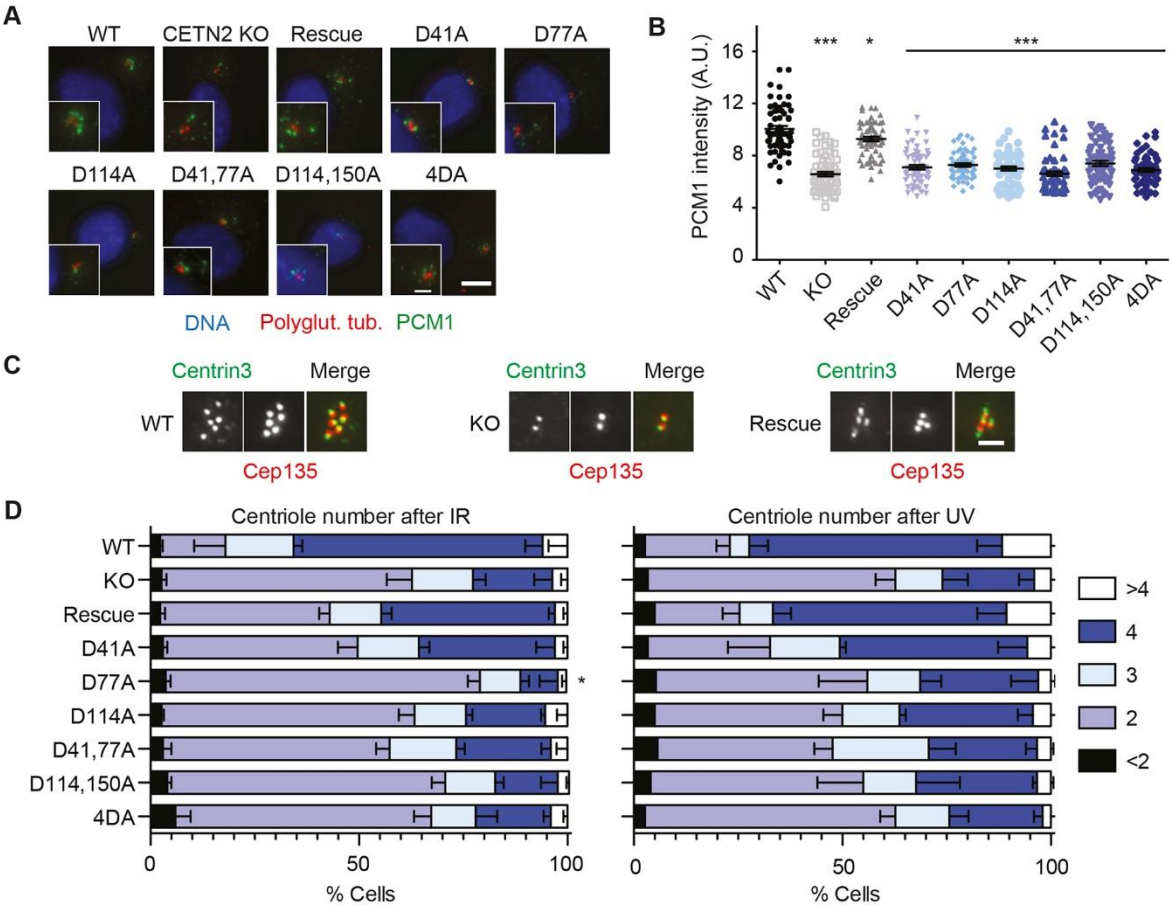

Figure 3 Centrin2 and its EF-hands are required for centriolar satellite localisation

A. Immunofluorescence micrograph showing the centriolar satellite localisation in wild-type cells and the indicated centrin2 mutant-expressing clones. Scale bar, 5 µm; inset scale bar, 2 µm.

B. Quantitation of PCM1 intensity within 30 μm^2 around the polyglutamylated tubulin centrosome signal after 18h serum starvation. A.U., arbitrary fluorescence units. Data show mean ± s.e.m. determined from 60 cells in 2 separate experiments. *, $P<0.05$, ***, $P<0.001$ compared to wild-type by ANOVA and Dunnett's multiple comparison test.

C. Immunofluorescence micrograph with the centriolar markers Cep135 and centrin3 to visualise centrosome numbers after 5Gy ionising radiation (IR) in wild-type, *CETN2* null and rescue cells. Images of >4, 2 and 4 centrioles are shown. Scale bar, 2 µm.

D. Quantitation of centriole numbers in cells of the indicated genotype 48h after 5Gy IR or 5J/m^2 UV irradiation, scored by microscopy image analysis of Cep135 and centrin3. Bar graph shows the mean $\pm$ s.d. of cells with the indicated number of centrosomes from 3 separate experiments in which at least 100 cells were quantitated. *, $P<0.05$ for the % of cells with centriole amplification (3 or >4) compared to controls by ANOVA and Dunnett's multiple comparison test.

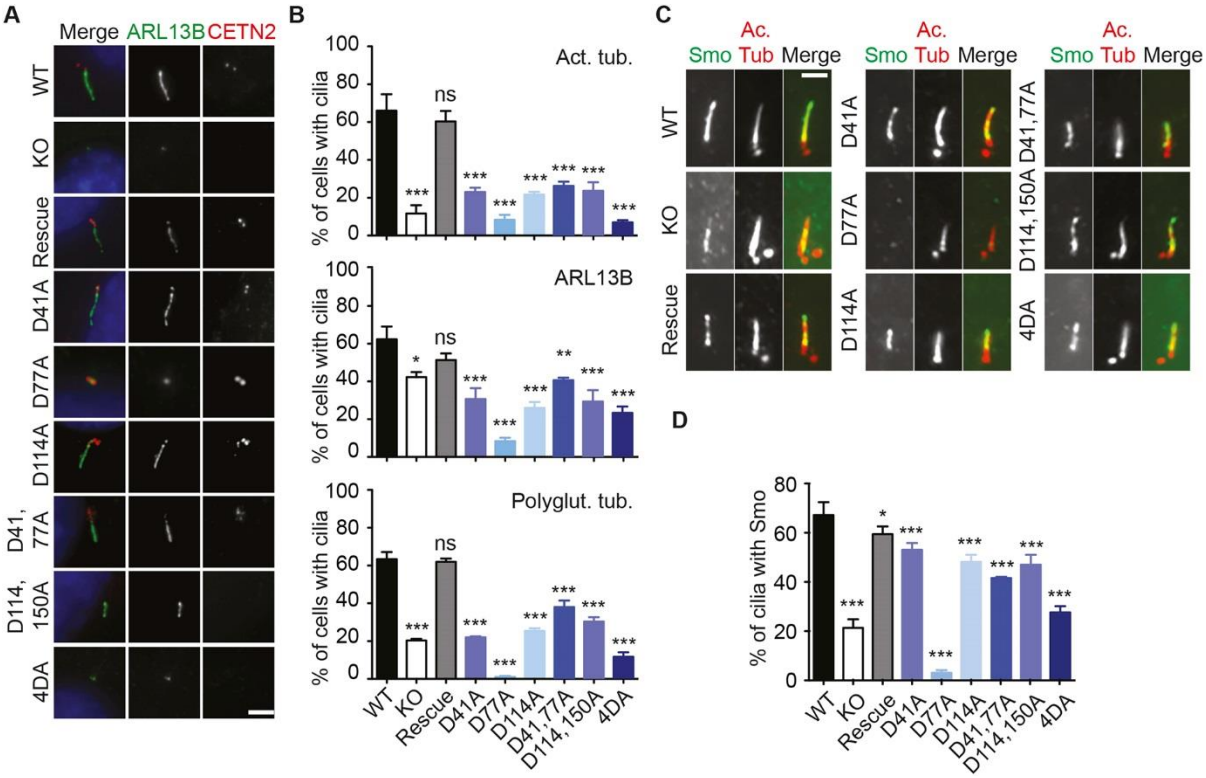

Figure 4 Defective ciliogenesis and ciliary function in centrin2-deficient and EF-hand mutant cells

A. Immunofluorescence micrograph showing representative images of ciliary structures observed in cells of the indicated genotype after 18h serum starvation. Scale bar, 5 µm.

B. Bar graphs show the mean percentage + s.e.m. of cells with cilia after 18h serum starvation, as determined by staining for the indicated ciliary marker, scored from 3 separate experiments in which at least 100 cells were counted. Ns, non-significant; **, $P<0.01$; ***, $P<0.001$ compared to wild-type by ANOVA and Dunnett's multiple comparison test.

C. Immunofluorescence micrograph showing Smo localisation to the cilium in cells of the indicated genotype. Cells were serum-starved for 48h, then treated with 100 nM SAG for 4h prior to fixation and analysis. Scale bar, 2 µm.

D. Bar graphs show the mean percentage + s.e.m. of ciliated cells with Smo localisation to the cilium, scored from 3 separate experiments in which at least 30 cilia were counted. *, $P<0.05$; ***, $P<0.001$ compared to controls by ANOVA and Dunnett's multiple comparison test.

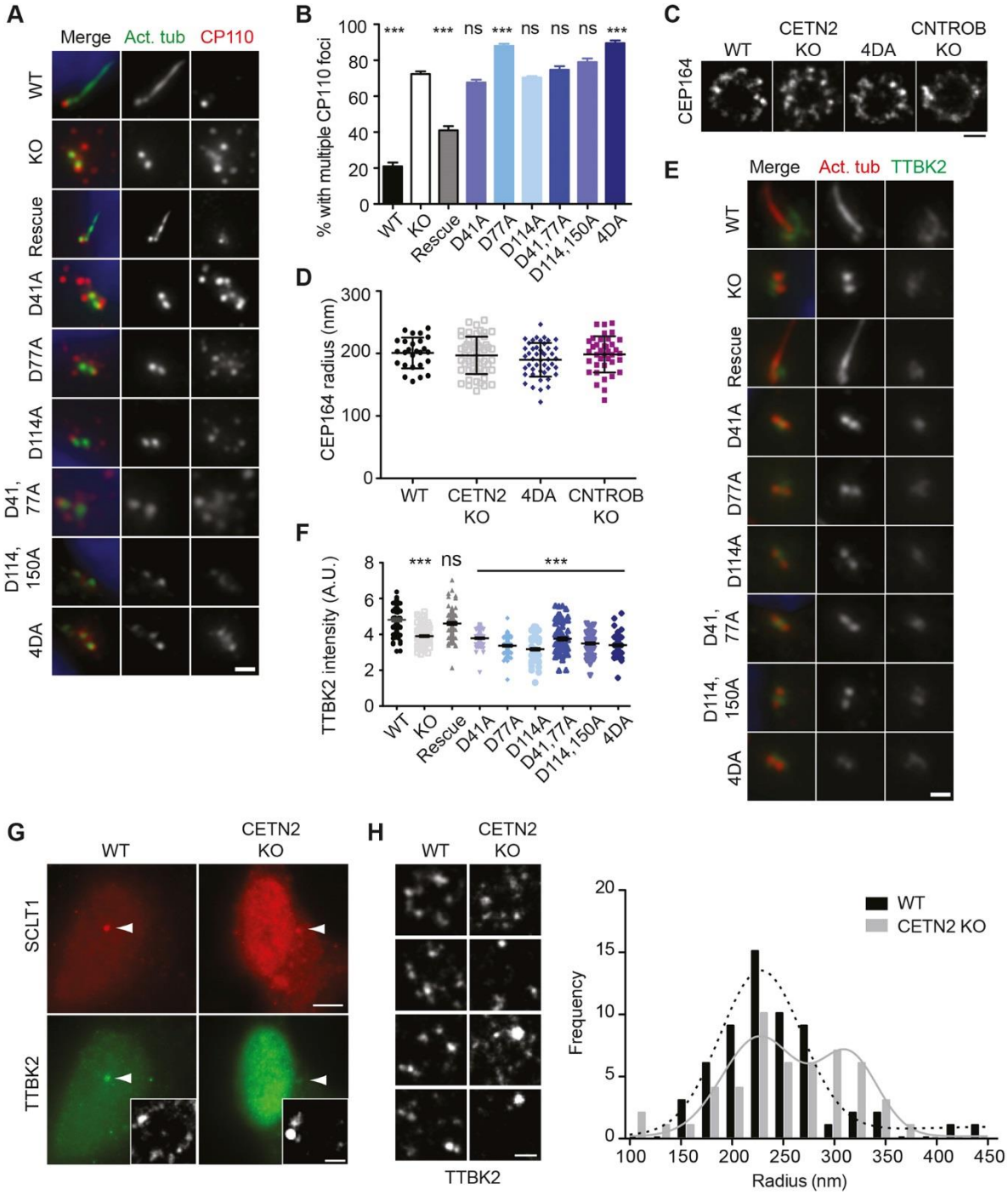

Figure 5 Centrin2 and its EF-hands are required for efficient removal of CP110 and appropriate localisation of TTBK2

A. Immunofluorescence micrographs showing representative images of CP110 localisation (red) around centrioles (acetylated tubulin, Act. Tub., green) in cells of the indicated genotype after 18h serum starvation. Scale bar, 2.5 µm.

B. Bar graphs show the mean percentage + s.e.m. of cells with multiple CP110 foci around centrioles after 18h serum starvation, scored from 3 separate experiments in which at least 100 cells were counted. Ns, non-significant; ***, $P<0.001$ compared to wild-type by ANOVA and Dunnett's multiple comparison test.

C. Representative dSTORM images showing the annular structures formed by CEP164 in cells of the indicated genotype. Scale bar, 200 nm.

D. Frequency plots of the radius of the CEP164 rings visualised by dSTORM in cells of the indicated genotype. Data show mean $\pm$ s.d. of at least 27 data points out of 3-4 centrioles.

E. Immunofluorescence micrographs of TTBK2 (green) localisation around centrioles/ basal bodies (red). Scale bar: 2 µm.

F. Dot plots of TTBK2 intensity measurements within a 30 μm^2 area around the centrosome. Plot shows data from 3 separate experiments in which 30 individual cells of the indicated genotype or centrin2 transgene expression were analysed. A.U., arbitrary units. Ns, non-significant; ***, $P<0.001$ compared to wild-type by ANOVA and Dunnett's multiple comparison test.

G. Immunofluorescence microscopy analysis of TTBK2 (green) and with Sclt1 (red) to confirm an axial orientation of the centriole (arrows) in hTERT-RPE1 cells of the indicated

genotype after 24h serum starvation. dSTORM axial views of TTBK2 are shown in the insets. Scale bar, 5 µm; inset scale bar, 200 nm.

H. (Left) dSTORM images showing the distribution patterns of TTBK2 in hTERT-RPE1 and centrin2 null cells after 24h serum starvation. Scale bar, 200 nm. (Right) Frequency distribution of the TTBK2 signal radius around Sclt1 in centrin2-deficient cells implies that TTBK2 is located in a more dispersed and random manner in the absence of centrin2.

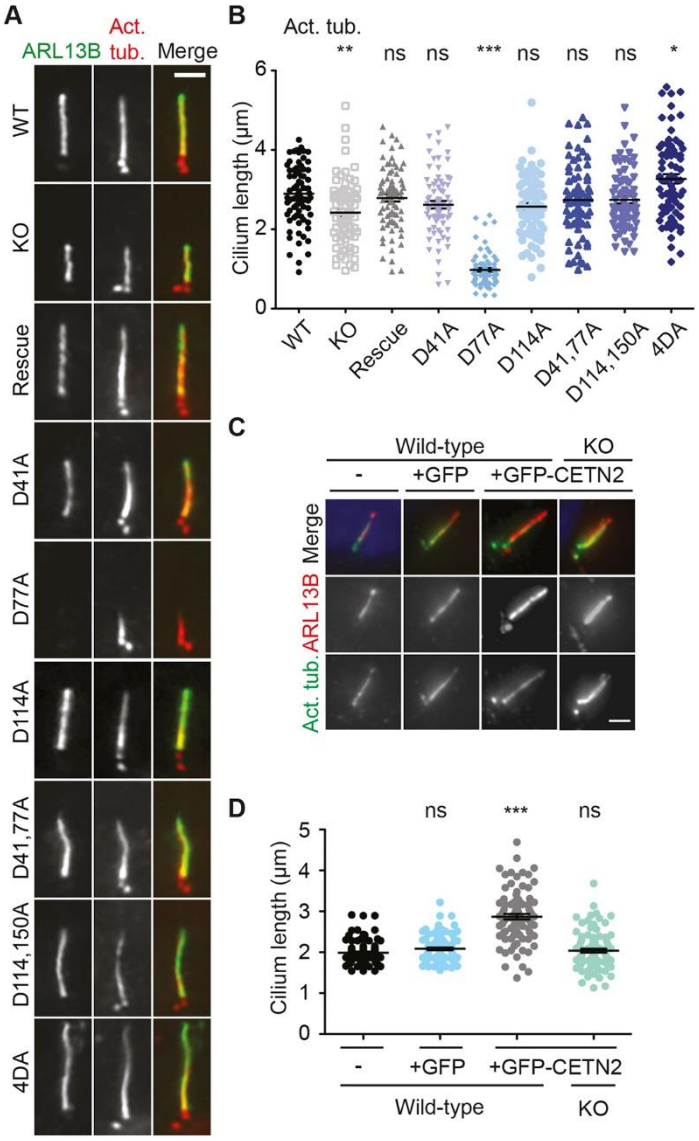

Figure 6 Centrin2 and its EF-hands affect primary cilium length

A. Immunofluorescence microscopy analysis of cilia using the indicated markers in cells of the indicated genotype. Scale bar, 2 µm.

B. Data show mean lengths ± s.d. from three independent experiments in which cilia were measured in 30 cells after 24h serum starvation using acetylated tubulin as a ciliary axoneme marker. ns, non-significant; *, $P<0.05$; **, $P<0.01$; ***, $P<0.001$ compared to wild-type by ANOVA and Dunnett's multiple comparison test.

C. Immunofluorescence microscopy analysis of cilia in cells transfected with the indicated GFP expression construct 24h prior to 18h serum starvation. Scale bar, 2 µm.

D. Data show mean lengths ± s.d. from three independent experiments in which cilia were measured in 30 cells using ARL13B as a ciliary axoneme marker. ns, non-significant; ***, $P<0.001$ compared to wild-type by ANOVA and Dunnett's multiple comparison test.

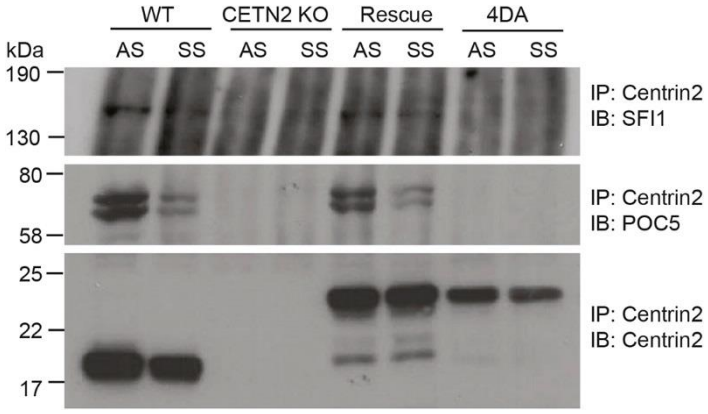

Figure 7 EF-hand dependent interaction of centrin2 with POC5 and SFI1

Lysates from wild-type cells and *CETN2* nulls with or without the indicated centrin2 transgene were immunoprecipitated ('IP') with antibodies to centrin2 and blotted with antibodies to the indicated protein ('IB').

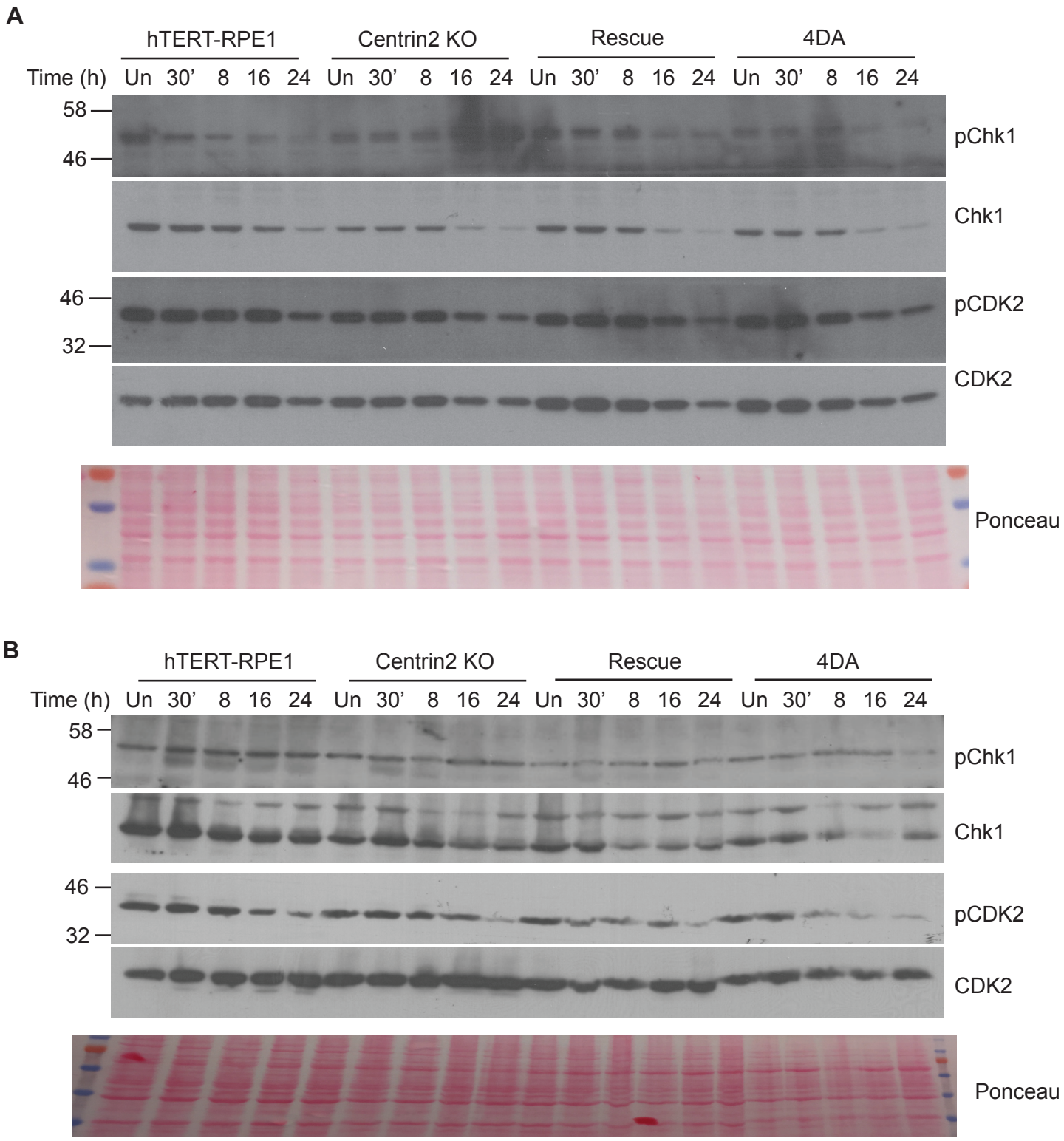

Supplementary Data

Figure S1

A. Immunoblot analysis of Chk1 and CDK2 phosphorylation in cells of the indicated genotype after IR treatment. Cells were treated with 5 Gy IR and CHK1 phosphorylation was visualised using anti-phospho-Chk1 S345 over the indicated timecourse. A blot for total Chk1 was used as a loading control. CDK2 phosphorylation was visualized with anti-phospho-CDK2 T160 and anti-CDK2. Ponceau was used as a loading control. Size markers are in kDa. Un, untreated control.

B. Immunoblot analysis of Chk1 and CDK2 phosphorylation in response to UV irradiation. Cells were treated with 5 J/m^2 UV treatment and analysed as for **A.**

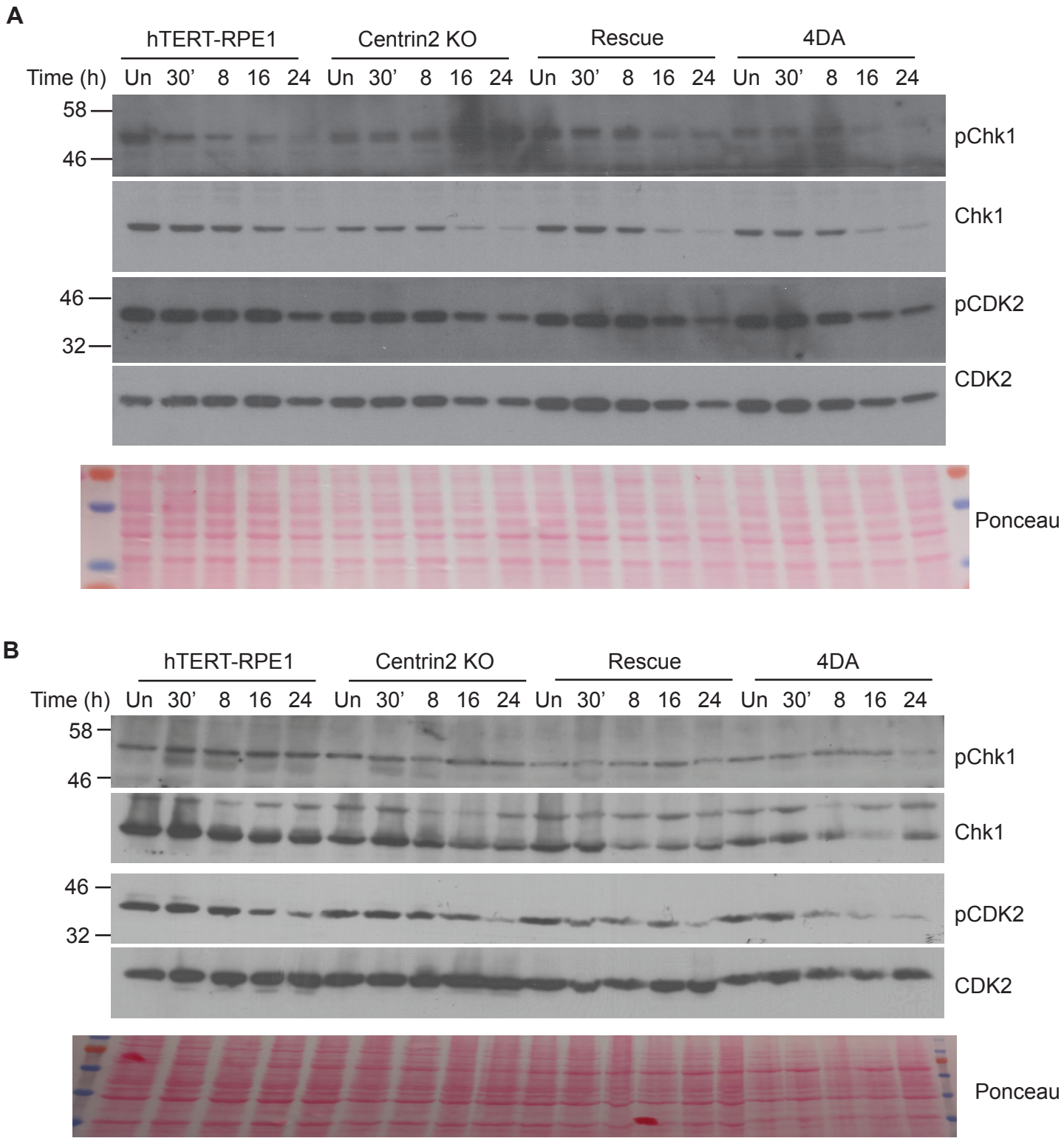

Supplementary Data

Figure S1

A. Immunoblot analysis of Chk1 and CDK2 phosphorylation in cells of the indicated genotype after IR treatment. Cells were treated with 5 Gy IR and CHK1 phosphorylation was visualised using anti-phospho-Chk1 S345 over the indicated timecourse. A blot for total Chk1 was used as a loading control. CDK2 phosphorylation was visualized with anti-phospho-CDK2 T160 and anti-CDK2. Ponceau was used as a loading control. Size markers are in kDa. Un, untreated control.

B. Immunoblot analysis of Chk1 and CDK2 phosphorylation in response to UV irradiation. Cells were treated with 5 J/m^2 UV treatment and analysed as for **A.**